pharmaceuticals

MDPI

Article

Enabling Irreversible FAP Inhibitors for Routine Clinical Use: Process and Quality Control Validation for [^{68}Ga]Ga-FAPi-mFS and [^{177}Lu]Lu-FAPi-mFS

Sarah Stephan [1,*], Subhadeep Paul [2], Sven Stadlbauer [2], Aleksandr Eismant [1], Rimos Lahdo [1], Christian Landvogt [1], Richard P. Baum [1] and Lukas Greifenstein [1,*]

[1] Curanosticum MVZ GmbH Wiesbaden-Frankfurt, Center for Advanced Radiomolecular Precision Oncology, 65191 Wiesbaden, Germany; eismant@curanosticum.de (A.E.); lahdo@curanosticum.de (R.L.); landvogt@curanosticum.de (C.L.); baumrp@gmail.com (R.P.B.)

[2] Helmholtz-Zentrum Dresden—Rossendorf, Institute of Radiopharmaceutical Cancer Research, 01328 Dresden, Germany; s.paul@hzdr.de (S.P.); s.stadlbauer@hzdr.de (S.S.)

* Correspondence: stephan@curanosticum.de (S.S.); greifenstein@curanosticum.de (L.G.)

Abstract

Background/Objectives: Fibroblast activation protein (FAP) represents an attractive target for both cancer imaging and radionuclide therapy. Nevertheless, the prolonged retention of many FAP-targeting inhibitors within tumor tissue remains challenging. Therefore, we investigated FAPi-mFS, an FAP inhibitor derived from FAPi-04 that carries a fluorosulfate warhead in meta position. This structural feature was designed to enable a predominantly irreversible covalent binding to FAP, thereby improving tumor retention time. **Methods**: [^{68}Ga]Ga-FAPi-mFS and [^{177}Lu]Lu-FAPi-mFS were successfully synthesized for large-scale clinical use by radiolabeling FAPi-mFS under validated conditions. The radiochemical conversion, yield, purity and stability were evaluated using radio-thin-layer chromatography (TLC), radio-high-performance liquid chromatography (HPLC), and in vitro human serum stability tests. **Results**: In the radiolabeling experiments, reproducibly high radiochemical purities of over 96% were achieved for both nuclides, along with decay-corrected yields of over 90% for gallium-68 (Ga-68) and over 80% for lutetium-177 (Lu-177) for batch sizes for Lu-177 up to 50 GBq. Both radiopharmaceuticals exhibited high in vitro stability with minimal release of Ga-68 (<1%) over 90 min and Lu-177 (<11%) over two physical half-lives. **Conclusions**: FAPi-mFS can be efficiently labeled with both Ga-68 and Lu-177 with high purity and stability using clinically applicable procedures. As a covalent FAP inhibitor, FAPi-mFS represents a promising strategy for prolonging retention time in tumors and potentially enhancing the therapeutic efficacy of FAP-specific radiopharmaceuticals.

Keywords: fibroblast activation protein (FAP); covalent targeted radioligand (CTR); sulfur(VI) fluoride exchange (SuFEx) chemistry; gallium-68 (Ga-68); Lutetium-177 (Lu-177); process validation; radiopharmaceutical; radionuclide therapy; theranostics

Check for updates

Academic Editors: Hirofumi Hanaoka, Ute Hennrich and Martina Benešová-Schäfer

Received: 7 October 2026
Revised: 21 October 2026
Accepted: 26 October 2026
Published: 29 October 2026

Copyright: © 2026 by the authors. Licensee MDPI, Basel, Switzerland. This article is an open access article distributed under the terms and conditions of the Creative Commons Attribution (CC BY) license.

1. Introduction

Over recent years, fibroblast activation protein (FAP) has gained significant traction as an important target for diagnostic positron emission tomography (PET). As a type II transmembrane serine protease, this enzyme features distinct dipeptidyl and endopeptidase activities that underpin its clinical utility [1,2]. FAP exhibits both dipeptidyl peptidase and endopeptidase activities, enabling the cleavage of specific dipeptides from the N-terminus

of peptide substrates and the degradation of extracellular matrix components, respectively. These enzymatic functions support processes associated with tissue remodeling and tumor progression [2]. Importantly, FAP is highly expressed on the surface of cancer-associated fibroblasts (CAFs), which are abundant in the tumor microenvironment of many solid malignancies, whereas its expression in most healthy adult tissues is comparatively low [3–5]. This differential expression, together with the accessibility of FAP on the cell surface, makes it an attractive molecular target for radiopharmaceuticals. FAP-targeting radioligands can selectively bind to FAP-expressing stromal cells and thereby enable the accumulation of radioactive tracers within the tumor microenvironment, providing a basis for both molecular imaging and targeted radionuclide therapy [6].

Using the small molecule (S)—N-(2-(2-cyano-4,4-difluoropyrrolidin-1-yl)-2-oxoethyl)quinoline-4-carboxamide (UAMC1110), a highly potent, selective FAP inhibitor first presented by Jansen et al., established the chemical basis for the development of the most widely used FAP inhibitors so far [1,7]. Based on this structure and through the addition of a bifunctional chelating agent, numerous radioactively labelable derivatives have been developed [8,9]. One of the first derivatives is FAPi-04, which exhibits high affinity, rapid and high tumor uptake, and rapid renal excretion. It was the first compound to demonstrate excellent in vivo tumor-to-background ratios across a wide range of solid tumors [10,11]. Subsequent linker optimizations led to the development of FAPi-46, which shows slightly better tumor retention and slower blood clearance [12–16]. With prolonged tumor residence times for therapies in MinD dimerization of FAPi derivatives, such as in DOTA-(SA.FAPi)$_2$ and DOTAGA-(SA.FAPi)$_2$ synthesized by Moon et al. or BiOncoFAP-DOTAGA by Galbiati et al., also led to enhanced tumor uptake and retention time in the tumor [17–22]. Compared to the corresponding monomeric and dimeric derivatives, trimerization such as in OncoFAP-23 led to a further increase in FAP affinity [23]. In addition, albumin-binding conjugated FAP structures such as TEFAPI-06, TEFAPI-07, FAPi-Ibu (integrating ibuprofen) and FAPi-EB (integrating Evans blue) were developed to improve the pharmacokinetics of FAPi radiopharmaceuticals, which again demonstrated increased tumor uptake and longer retention compared to therapeutic FAPi-04 [24–26]. Another approach involved the peptide-based FAP-2286 and 3BP-3940, which exhibited longer tumor retention, stability, and accelerated blood clearance [27–32]. Despite these advances, all of the aforementioned FAP tracers bind reversibly to the enzyme, which may still limit their residence time in tumor tissue.

However, to increase the therapeutic tumor dose, it would be highly beneficial if the radiopharmaceutical remained in the tumor environment for an even longer period. The concept of covalently binding FAP inhibitors (CTRs) was first applied by Cui et al. In this approach, aryl fluorosulfate-based "latent warheads" serve as reactive groups that can covalently react specifically with nucleophilic amino acids in the active site of FAP. Sulfur(VI) fluoride exchange (SuFEx) chemistry was employed for this purpose [33]. Starting from FAPi-04 (Figure 1A), a derivative was developed that carries an FS warhead. This so-called FAPi-mFS (Figure 1B) includes this FS warhead in a meta position and binds mostly irreversibly in the binding pocket of FAP, forming a covalent bond, and thus exhibits significantly prolonged tumor retention compared to its predecessors (Figure 1C).

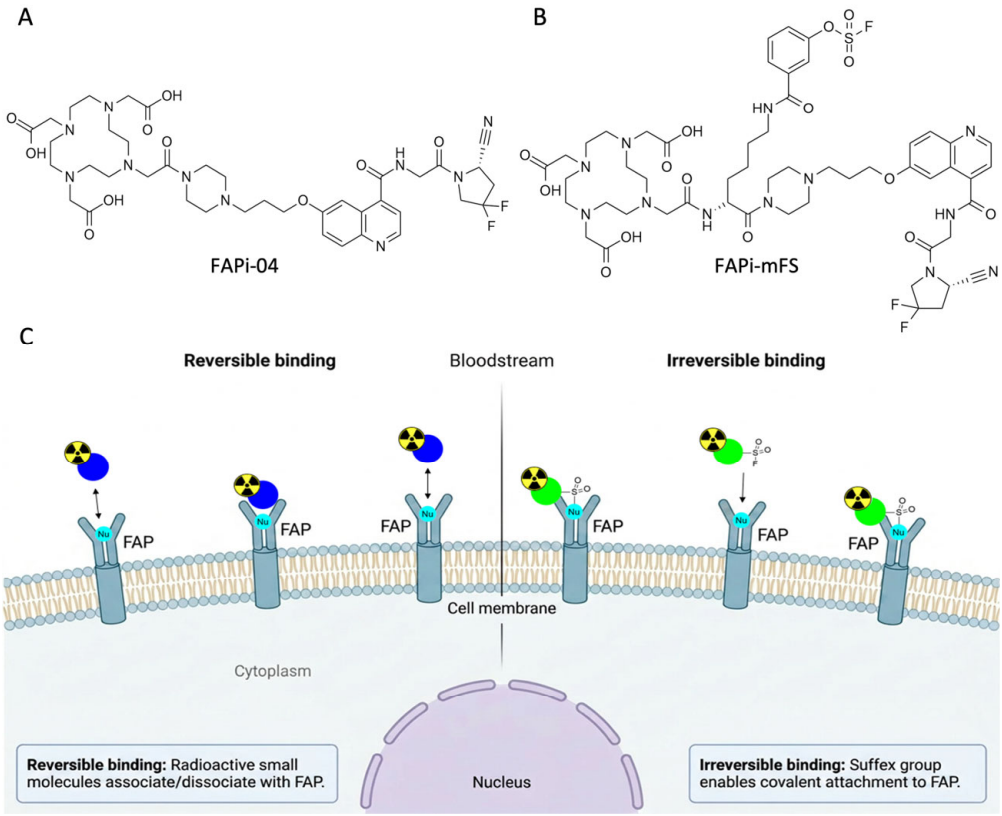


Figure 1. (**A**) Structure of FAPi-04. (**B**) Structure of FAPi-mFS. (**C**) Different mechanisms of binding to FAP. FAPi-04 binds reversibly to FAP (on the left side), and the SuFEx function of FAPi-mFS enables an irreversible covalent bond, resulting in prolonged retention within the tumor (on the right side).

FAPi-mFS was initially investigated in preclinical studies using both cell models and mouse models. In a first step, a binding assay demonstrated the irreversible binding of FAPi-mFS, and subsequently cell uptake was assessed in HT-1080-FAP cells. The uptake of [^{68}Ga]Ga-FAPi-mFS was significantly higher than that of [^{68}Ga]Ga-FAPi-04. Furthermore, an efflux–retention assay demonstrated that FAPi-mFS, with a significantly prolonged half-life of cellular retention, remains in the cells for much longer than FAPi-04. In mouse models, [^{68}Ga]Ga-FAPi-mFS demonstrated significantly higher tumor uptake and better image contrast in HT-1080 FAP-bearing mice compared to [^{68}Ga]Ga-FAPi-04. Additionally, in vivo therapy experiments with ^{177}Lu- and ^{225}Ac-labeled FAPi-mFS resulted in substantial tumor inhibition, extending to complete tumor control in some treatment arms. Clinically, [^{68}Ga]Ga-FAPi-mFS was used in an initial, investigator-initiated pilot study in two patients with medullary thyroid carcinoma, where the tracer identified more suspicious lesions and demonstrated higher tumor-to-background ratios than [^{68}Ga]Ga-FAPi-04 [33,34].

Although FAPi-mFS has already been investigated in preclinical and early clinical trials, there has been no systematic description to date of its translation into a reproducible clinical production process. Robust automated labeling parameters, batch-to-batch consistency, validated analytical methods, and comprehensive quality control procedures are essential conditions for safe clinical use. To make these molecules accessible to a broader patient population, the aim of this paper therefore is to describe the automated radiolabeling of FAPi-mFS, its radiochemical stability, and the development and validation of the analytical radio-HPLC method for quality control in a clinical setup with the nuclides Ga-68 and Lu-177. For this purpose, the labeling conditions were optimized, process reproducibility was evaluated, and safe and compliant manufacturing of these radiopharmaceuticals was

demonstrated. This work thus provides a practical basis for the standardized clinical production of FAPi-mFS-based radiopharmaceuticals.

2. Results

2.1. Labeling Process Optimization, Validation and Quality Control of [^{68}Ga]Ga-FAPi-mFS

The radiolabeling of FAPi-mFS with gallium-68 was performed using an automated synthesis procedure on a mini all-in-one cassette-based module (Trasis, Figure 2A). The module was installed in an H700 hot cell and radiolabeling took place in a class C environment integrated into a non-controlled area, while the formulation of the final product was carried out in a closed class A isolator. During automated synthesis, the ^{68}Ge/^{68}Ga-generator (50 or 100 mCi) was eluted with 5 mL 0.1 M hydrochloric acid (HCl) through a syringe connected to position E of the cassette at an optimized flow rate of 1 mL/min. The resulting eluate is collected in syringe 3 and subsequently transferred into the orange reaction vial located in the center of Figure 2A. The precursor, previously dissolved in buffer, is then delivered from connection D into the reactor using syringe 3 by applying overpressure to vial D. After the heating phase, the reaction mixture is again taken up with syringe 3 and transferred via the HPLB+ cartridge in position 10, which retains the radiolabeled molecules, into the waste vial. The reactor is then rinsed by syringe 3 drawing 0.9% sodium chloride (NaCl) from connection 6, pressing it into the reactor, and after a short exposure transferring the solution again into the waste bottle via the cartridge. To elute the cartridge, syringe 3 draws 0.5 mL of ethanol from port B and passes it through the cartridge into the final product vial connected to the system. Finally, the cartridge is rinsed with 10 mL of 0.9% NaCl and the final product is formulated passing the sterile filter.

During process optimization, an ideal radiolabeling temperature of 85 °C was determined for [^{68}Ga]Ga-FAPi-mFS. Below a temperature of 85 °C a significant decrease in labeling yields was observed, while an increase in temperature to 95 °C led to increased formation of side products. These were presumably hydrolysis or decomposition products of the arylfluorosulfate group on the activated phenyl ring, whereby fluoride or fluorosulfonic acid derivatives split off to form a phenol or phenoxy sulfate side product, which is produced during heating (Figure 2F). However, due to the small amount of the radioactive side product formed and the limited availability of sufficient material for isolation and subsequent LC-MS or HRMS analysis, it was not possible to definitively identify their structure in this study. It is highly important here to pay close attention to a robust HPLC setup and a shallow gradient, as the side products otherwise may not be separated sufficiently. For the kinetics, the labeling reaction was investigated at 95 °C with different amounts of precursor (1, 2, 5 and 10 nmol) using starting activities between 47 and 50 MBq for each reaction. The kinetics (Figure 2E) showed that reducing the amount of precursor led to a reduction in yield. The fastest reaction was observed at 10 nmol within 10 to 15 min, although the 5 nmol solution also achieved complete conversion after 25 min.

For routine labeling, 50 µg of FAPi-mFS in sodium acetate buffer (1.0 M, pH 5.5, 2 mL) was heated to 85 °C for 12 min, resulting in a decay-corrected radiochemical yield (RCY) of approximately 90%. For robust routine production, these optimized process parameters are applied as part of process validation (n = 3) at initial activities between 419 and 465 MBq. The validation focuses on two main acceptance criteria: radiochemical purity (RCP) of >95% (determined by radio-HPLC) and an RCY of >80%. A representative analytical radio-HPLC chromatogram is shown in Figure 2B, indicating an RCP of 98.6%. In addition to the desired product peak, the HPLC chromatogram shows an additional major radioactive side product with a retention time of t_R = 3.25 min (main peak t_R = 3.98 min) (Figure 2B). Validation of the analytical HPLC method confirmed effective separation of the radiotracer from this impurity, enabling its quantification. The side product was typically

observed at a proportion of approximately 1–2%. The mean RCP of the validation runs was 98.8 ± 0.12%, with a mean RCY of 92.4 ± 3.0%, which demonstrates that the process can be operated efficiently and robustly within these specifications. Furthermore, molar activity lay in the range of 10.1 to 11.2 MBq/nmol. Routine syntheses on the generator afforded final activities of 510–640 MBq, corresponding to decay-corrected radiochemical yields of approximately 90% based on the initial generator eluate activities of 710–880 MBq.

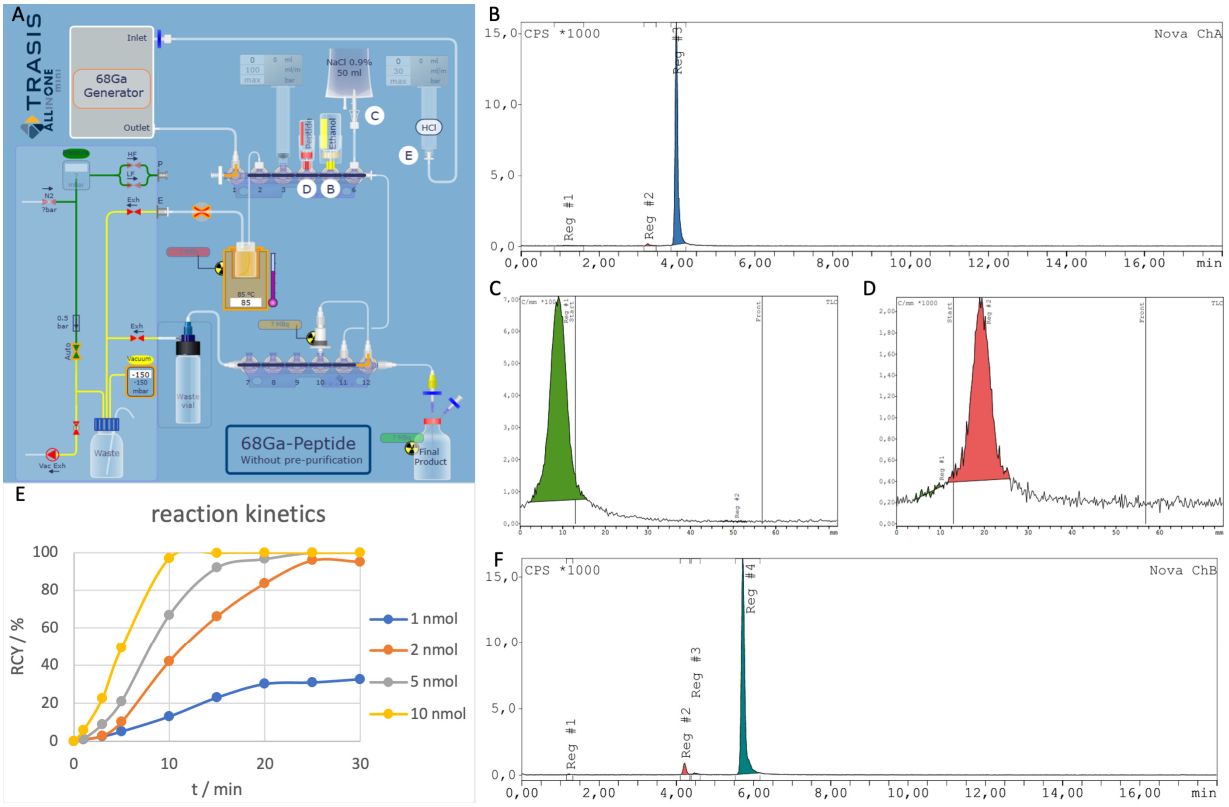


Figure 2. (**A**) Overview of the synthesis setup for the production of [^{68}Ga]Ga-FAPi-mFS. (**B**) Radio-HPLC chromatogram of [^{68}Ga]Ga-FAPi-mFS, where the desired product peak has a t_R of 3.98 min and the peak of the major side product a t_R of 3.25 min (method: gradient from 10% to 20% acetonitrile (MeCN) + 0.1% trifluoroacetic acid (TFA) in 10 min). Radio-TLC of [^{68}Ga]Ga-FAPi-mFS in citrate acid buffer (**C**) and in 1 M ammonium acetate–methanol buffer (**D**) with no relevant amounts of free Ga-68. (**E**) Reaction kinetics at 95 °C with different amounts of precursor (1, 2, 5 and 10 nmol). (**F**) Radio-HPLC chromatogram of [^{68}Ga]Ga-FAPi-mFS after 15 min at 95 °C with an RCP of 95.2%. For better presentation, a different method was used (gradient from 5% to 45% MeCN + 0.1% TFA in 10 min).

In addition to determining radiochemical purity by HPLC, the result was verified using a dual-TLC system (Figure 2C,D), which gave further insight into the presence of colloidal gallium. Furthermore, quality control includes the determination of the dose activity, a visual inspection, measurement of the pH value, gamma spectrometry for nuclide identification and determination of the physical half-life, sterile filter integrity testing and endotoxin analysis. Table 1 summarizes the specifications and the corresponding quality control results. All values during process validation fall within the specified acceptance limits and ensure the provision of a pharmaceutical product of appropriate quality.

Table 1. An overview of the quality control tests performed and the specifications for the validations of [^{68}Ga]Ga-FAPi-mFS and [^{177}Lu]Lu-FAPi-mFS. TLC I is in citrate acid buffer and TLC II is in 1 M ammonium acetate/methanol buffer.

	[^{68}Ga]Ga-FAPi-mFS	[^{177}Lu]Lu-FAPi-mFS	Specifications
Color	Colorless	Colorless	Colorless
pH	4.5	3.5–4.0	3.5–7.5
TLC I	98.6 ± 0.7%	99.3 ± 0.1%	>95%
TLC II	99.9 ± 0.2%	99.9 ± 0.1%	>95%
HPLC	98.8 ± 0.1%	97.9 ± 0.6%	>95%
Endotoxin	<5.0 EU/mL	<5.0 EU/mL	<17.5 EU/mL
Bubble point	>2500 mbar	>2500 mbar	>2500 mbar
Radionuclide impurity	<0.01%	<0.001%	<0.01%

2.2. Labeling Process Optimization, Validation and Quality Control of [^{177}Lu]Lu-FAPi-mFS

The radiolabeling of FAPi-mFS with Lu-177 was carried out in a fully automated process using a mini All-in-One cassette module (Trasis), as described in the previous section. In the automated Lu-177 radiolabeling procedure, the V-shaped vial containing Lu-177 is connected with two cannulas, a short cannula at position 1 and a longer one connected to the orange reactor in Figure 3A. The synthesis is initiated by syringe 3, which generates overpressure in vial A and thereby transfers its contents into the reactor. The pecursor, which has been dissolved in buffer, is then aspirated from port B into vial A using syringe 3 and transferred into the orange reactor. After the heating phase, syringe 3 draws 5 mL of 0.9% NaCl solution from port C and collects the entire reactor contents into syringe 3 for dilution. The resulting mixture is passed through the integrated sterile filter into the final product vial. Finally, syringe 3 rinses the reactor twice with 4 mL of 0.9% NaCl solution each time, with both rinses also being transferred to the final product vial.

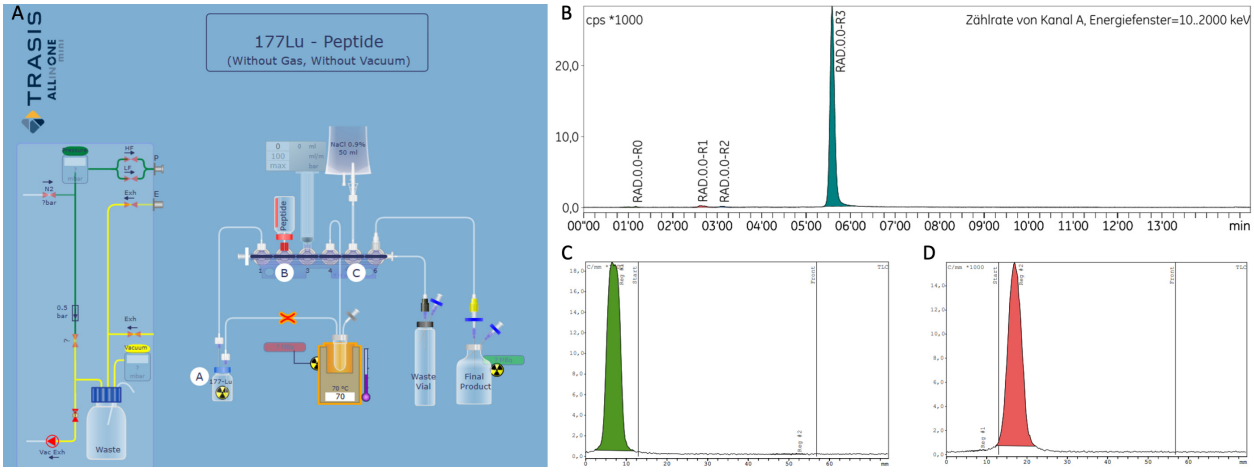


Figure 3. (**A**) Overview of the synthesis setup for the production of [^{177}Lu]Lu-FAPi-mFS. (**B**) Radio-HPLC chromatogram of [^{177}Lu]Lu-FAPi-mFS, where the main peak has a t_R of 5.35 min and the peak of the main side product a t_R of 2.38 min (method: gradient from 20% to 45% MeCN + 0.1% TFA in 10 min). Radio-TLC of [^{177}Lu]Lu-FAPi-mFS in citrate acid buffer (**C**) and in 1 M ammonium acetate/methanol buffer (**D**) with no relevant amounts of free Lu-177.

Radiolabeling was carried out in 0.6 M ascorbic acid solution with the addition of gentisic acid and L-methionine (1.2 mL, pH 4.5, 30 mg gentisic acid, 20 mg L-methionine) to minimize radiolysis. Process optimization identified a temperature gradient as the

optimal condition: 10 min at 70 °C followed by 40 min at 50 °C. Isothermal conditions at higher temperatures (e.g., 85 °C for 40 min) led to excessive formation of side products comparable to the ^{68}Ga-process (Figure S1). It is noteworthy that these reactions seem to be very stable at lower activity concentrations. However, using activity concentrations higher than 2 GBq/mL led to substantial side-product formation that again was only detectable using a robust HPLC setup with shallow gradient.

Using these parameters, a process validation (n = 3) was carried out again, in which 40–50 µg of precursor per GBq and initial activities of between 7 GBq and 24 GBq were used. Further purification steps were unnecessary, as the final product fulfilled the predefined acceptance criteria, including radiochemical purity exceeding 95% (by radio-HPLC) and a radiochemical yield above 80%. An example of analytical radio-HPLC is shown in Figure 3B. The validation process yielded a mean RCP of 97.3 ± 0.9% and mean RCY of 89.2 ± 2.3%. For the subsequent routine productions (n = 9), quantities between 18 GBq and 53 GBq were used, resulting in a mean RCP of 97.9 ± 0.6% and a mean yield of 91.4 ± 3.9%. Just as in the HPLC chromatogram of [^{68}Ga]Ga-FAPi-mFS, a comparable side product is detectable in the chromatogram of [^{177}Lu]Lu-FAPi-mFS (Figure 3B). An overview of the quality control tests performed and the specifications are presented in Table 1. In addition to determining radiochemical purity by HPLC, this was also verified using a dual-TLC system (Figure 3C,D). Furthermore, the quality control included a visual inspection, pH determination, determination of the physical half-life for radionuclide identification, testing of sterile filter integrity and an endotoxin test. All results fell within the predefined specification limits and ensured the manufacture of a medicinal product of appropriate quality.

2.3. In Vitro Stability

Stability measurements were performed both in the formulation solution (pure) and in human serum (HS) to simulate relevant conditions. All samples were prepared in triplicate, incubated at 37 °C and analyzed by TLC. For ^{68}Ga-labeled compounds, measurements were taken over a period of 90 min, while ^{177}Lu-labeled analogs were studied over 14 days (Figure 4). In this context, ^{68}Ga exhibited very high stability of over 99%, while the ^{177}Lu-labeled compounds also showed stability of over 89% purity and in HS throughout the entire period.

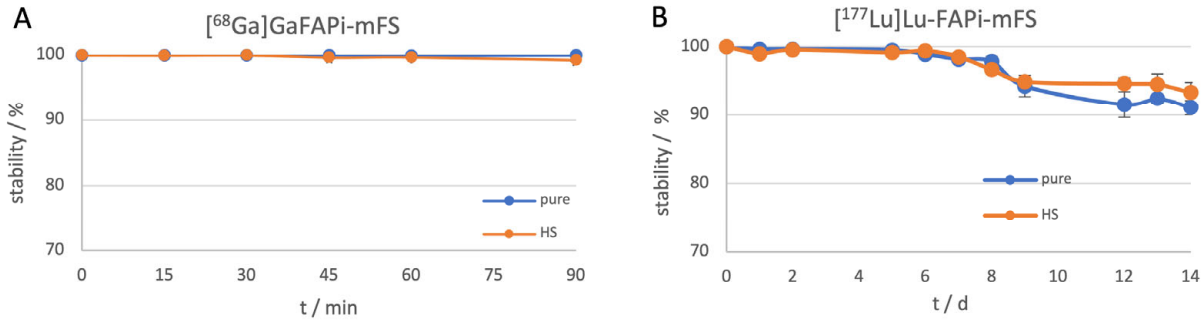


Figure 4. (**A**) Stability of [^{68}Ga]Ga-FAPi-mFS and (**B**) [^{177}Lu]Lu-FAPi-mFS in formulation (pure) and in human serum (HS) incubated at 37 °C, controlled by TLC.

2.4. HPLC Method Validation

The early development and validation of an efficient and robust HPLC method for quality control is essential when working with an initially unknown molecule. The experimental design and method optimization were conducted in accordance with the Conference for Harmonisation (ICH) and the EANM guideline [35]. For comprehensive validation, parameters such as linearity, accuracy, precision and specificity, in addition to the lower limit

of detection (LLOD) and the lower limit of quantification (LLOQ), were examined. For this purpose, [^{68}Ga]Ga-FAPi-mFS and [^{177}Lu]Lu-FAPi-mFS were used, as well as their inactive standards, analyzed via radioactivity and UV detection. Additionally, the carryover effect of the radioactivity detector was determined.

2.4.1. Linearity (Radioactivity Detection)

For [^{68}Ga]Ga-FAPi-mFS, a total of 15 measurements were performed using different activity levels ranging from 0.075 MBq to 1.25 MBq to plot the linearity curve for the radioactivity detector (Figure 5). Additionally, for [^{177}Lu]Lu-FAPi-mFS a total of five different activity concentrations ranging from 2.5 MBq to 12.5 MBq were measured in triplicate to determine the linearity for the radioactivity detector (Figure 5). In accordance with the requirements of the EANM guideline, the R^2 value for both molecules was higher than 0.99.

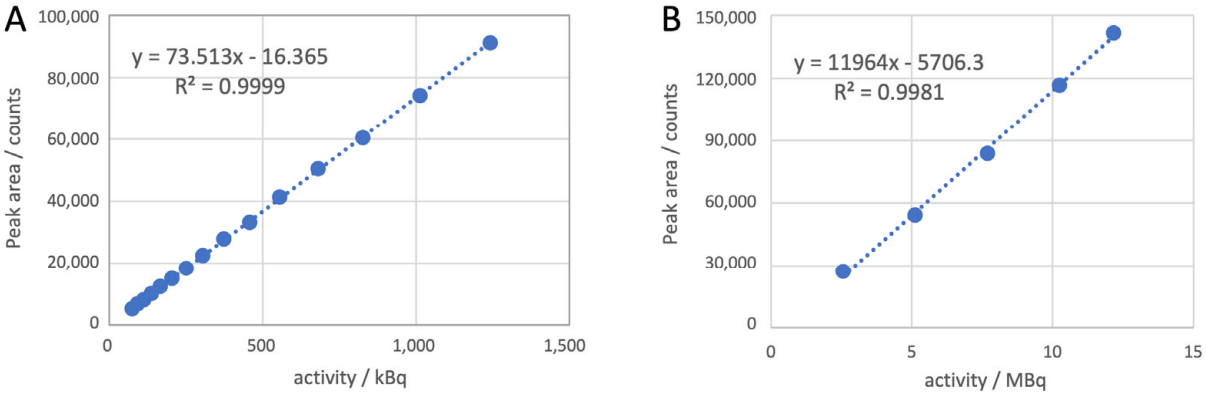


Figure 5. (**A**) Linearity of [^{68}Ga]Ga-FAPi-mFS for radiodetector with the linear equation y = 73.513x − 16.365 and R^2 = 0.9999 on the left. (**B**) [^{177}Lu]Lu-FAPi-mFS for radiodetector with the linear equation y = 11,964x − 5706.3 and R^2 = 0.9981 on the right.

2.4.2. Accuracy (Radioactivity Detection)

For accuracy testing consistent with the routine preparations, samples were diluted prior to measurement to ensure an appropriate activity concentration for HPLC analysis. Here, the samples were diluted 1:3 prior to HPLC analysis, resulting in an activity of 0.4 MBq in the 0.04 mL HPLC sample from the expected average radioactivity concentration of 40 MBq/mL. A total of twelve different measurements were performed at different Ga-68 radioactivity concentrations ranging from 25% to 225% of the expected reference activity (decay correction was performed in each case relative to the injection time). The recovery was between 97.04% and 99.40%, which complies with the requirements of the EANM guideline. In the absence of a calibrated reference source or an alternative HPLC system, the true value was determined based on linearity, taking decay correction into account.

As with Ga-68, routine samples of Lu-177 were also diluted to ensure an appropriate activity concentration for HPLC analysis. Similarly, the samples for the accuracy test were diluted, resulting in activities ranging from 2.5 MBq to 12.5 MBq in the HPLC samples. A total of ten different measurements were performed at five different ^{177}Lu radioactivity concentrations ranging from 30% to 160% of the expected reference activity (in each case, a decay correction relative to the injection time was applied). The accuracy for all concentrations ranged between 96.25% and 108.75%, which meets the requirements. Similarly to Ga-68, the true value was determined based on linearity, taking decay correction into account.

2.4.3. Precision (Radioactivity Detection)

Due to the difficulties involved in accurately reproducing radioactivity concentrations with Ga-68, eight samples with different concentrations were analyzed. The mean recovery rate for all measurements was less than 1% relative standard deviation (RSD) and thus complies with the requirements of the ICH guideline.

To assess the precision of [^{177}Lu]Lu-FAPi-mFS, six determinations were performed at 100% of the target concentration. The average recovery rate for all measurements was less than 1% RSD, thereby meeting the requirements.

2.4.4. Lower Limit of Detection (LLOD) and Lower Limit of Quantification (LLOQ) (Radioactivity Detection)

According to the guidelines, the LLOD and LLOQ can be determined using different methods, including visual inspection, signal-to-noise ratio measurement, or calculation based on the calibration curve. In this case, the calibration curve method was selected. For this purpose, $\sigma = 7.83\ \frac{1}{s}$ was used for the standard deviation of the calibration curve and $m = 73.51\ \frac{1}{s} \cdot \frac{\mu L}{kBq}$ for the slope of the curve for the ^{68}Ga compound.

$$LLOD = \frac{3.3\sigma}{m} = \frac{3.3 \cdot 7.83\ counts}{73.51\ counts \cdot \frac{\mu L}{kBq}} = 0.35\ \frac{kBq}{\mu L} \quad (1)$$

$$LLOQ = \frac{10\sigma}{m} = \frac{10 \cdot 7.83\ counts}{73.51\ counts \cdot \frac{\mu L}{kBq}} = 1.06\ \frac{kBq}{\mu L} \quad (2)$$

For the ^{177}Lu compound, $\sigma = 2291.23\ \frac{1}{s}$ was used for the standard deviation of the calibration curve and $m = 11{,}963.98\ \frac{1}{s} \cdot \frac{\mu L}{kBq}$ for the slope of the curve, which resulted in an LLOD of 0.63 $\frac{kBq}{\mu L}$ and an LLOQ of 1.91 $\frac{kBq}{\mu L}$.

2.4.5. Carryover

After 15 consecutive measurements of [^{68}Ga]Ga-FAPi-mFS and also after six consecutive measurements of [^{177}Lu]Lu-FAPi-mFS, no significant carryover was observed in either the UV or the radioactivity detector channel (Figures S4 and S5). As no quantifiable carryover of radioactive species to the next run was detected, it was not necessary to carry out additional column flushes.

2.4.6. Linearity of Cold Standards (UV Detection)

For the HPLC identity test, a concentration of [^{nat}Ga]Ga-FAPi-mFS higher than the actual concentration expected in the final radiopharmaceutical product was used. This was necessary because the analytical concentration of the cold standard under routine synthesis conditions is close to or in some cases below the reliable detection or quantification limit of the UV/DAD detector. The chosen standard concentration ensures a clearly detectable, reproducible and unambiguously assignable reference peak. This allows the retention time and, where applicable, the UV spectrum of the reference standard to be reliably compared with the product peak. The higher concentration therefore serves solely to ensure the specificity, peak identification and reproducibility of the analytical method.

To determine the linearity curve for the UV detector for the two cold standards, five different molar quantities were measured in triplicate for each compound. For [^{nat}Ga]Ga-FAPi-mFS, five different amounts of substance in the range of 500 µg to 2400 µg and for [^{nat}Lu]Lu-FAPi-mFS in the range of 50 µg to 240 µg were used (Figure 6). In accordance with the requirements of the EANM guideline, the R^2 value for both molecules was higher than 0.99.

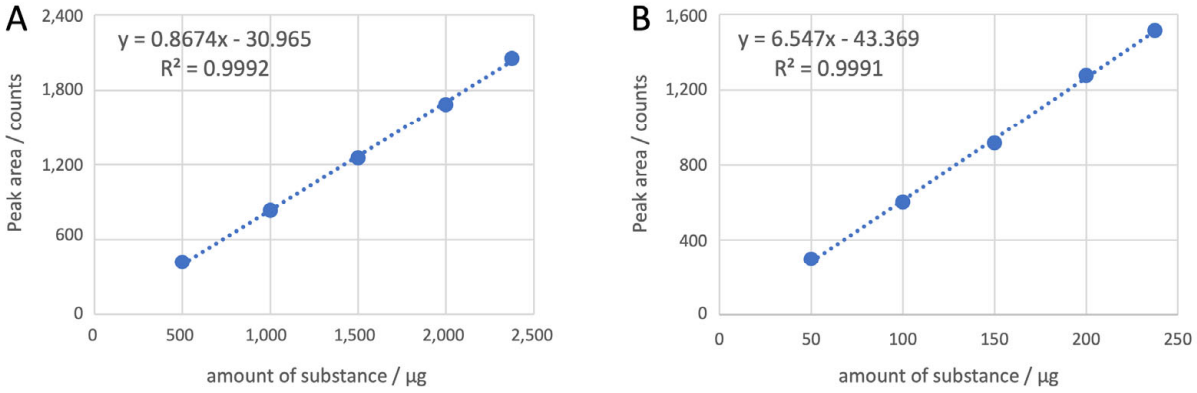


Figure 6. (**A**) Linearity of [^{nat}Ga]Ga-FAPi-mFS for UV detector with the linear equation y = 0.8674x − 30.965 and R^2 = 0.9992 on the left side. (**B**) Linearity of [^{nat}Lu]Lu-FAPi-mFS for with the linear equation y = 6.547x − 43.369 and R^2 = 0.9991 on the right.

2.4.7. Accuracy of Cold Standards (UV Detection)

Ten different measurements were performed at five different concentration levels for the two cold standards. All of them fell within the range of 30% to 160% of the expected concentration. The accuracy for all concentrations ranged between 90% and 110%, which meets the requirements.

2.4.8. Precision of Cold Standards (UV Detection)

For each of the two cold standards, six measurements were carried out at 100% of the expected concentration. The retention times and peak areas were measured and compared. The RSDs calculated for all measurements were below 1%, thereby meeting the requirements specified in the guidelines.

2.4.9. Lower Limit of Detection and Lower Limit of Quantification of Cold Standards (UV Detection)

Similar to the determination of the LLOD and LLOQ for radioactive compounds, the calculation for each cold standard was performed using the calibration curve. For [^{nat}Ga]Ga-FAPi-mFS, σ = 24.13 $\frac{1}{s}$ was used for the standard deviation of the calibration curve and m = 1.15 $\frac{1}{s} \cdot \frac{\mu L}{\mu g}$ for the slope of the curve.

$$LLOD = \frac{3.3\sigma}{m} = 69.12\ \frac{\mu g}{\mu L} \quad (3)$$

$$LLOQ = \frac{10\sigma}{m} = 209.46\ \frac{\mu g}{\mu L} \quad (4)$$

For [^{nat}Lu]Lu-FAPi-mFS, σ = 17.10 $\frac{1}{s}$ was used for the standard deviation of the calibration curve and m = 6.55 $\frac{1}{s} \cdot \frac{\mu L}{\mu g}$ for the slope of the curve, which resulted in an LLOD of 8.62 $\frac{\mu g}{\mu L}$ and an LLOQ of 26.12 $\frac{\mu g}{\mu L}$.

2.4.10. Specification

The retention time of the unlabeled peptide FAPi-mFS was compared with that of [^{nat}Ga]Ga-FAPi-mFS. Simultaneous injection of both molecules resulted in baseline separation with a t_R of 4.95 min for FAPi-mFS and 4.00 min for [^{nat}Ga]Ga-FAPi-mFS (Figure S2). These retention times were confirmed by the separate injection of the two compounds.

Since a different HPLC method was used for [^{177}Lu]LuFAPi-mFS, the retention time of the unlabeled peptide FAPi-mFS was t_R = 4.50 min and for [^{nat}Lu]LuFAPi-mFS t_R = 5.29 min, resulting in baseline separation (Figure S3).

3. Discussion

When introducing new radioactively labeled compounds for clinical trials, a detailed quality analysis is required to ensure the safe administration of the final product to patients. It is important that the drug is manufactured reproducibly and that only qualified equipment and validated procedures be used to ensure compliance with applicable regulations for the protection of patient safety. In addition, safe working conditions for operating personnel when handling radioactivity are of great importance. By implementing an automated manufacturing process instead of a manual one, radiation exposure for operating personnel was minimized and a reproducible production process was ensured [36,37]. The synthesis of the two radiopharmaceuticals, [^{68}Ga]Ga-FAPi-mFS and [^{177}Lu]Lu-FAPi-mFS, was successfully carried out on Trasis's automated mini-All-in-One synthesis module. This module was equipped with cGMP-compliant software (Trasis Suite Software—Version 2.35) and sterile, single-use materials of GMP quality, all housed in a shielded hot cell during radiolabeling. Both drug products were filled through a sterile filter into a closed sterile vial in a Class A isolator. Prior to use, quality control was performed, which included a filter integrity test, a test for bacterial endotoxins, and other methods for assessing the suitability of the drug products for human use. The tests presented in Table 1 were carried out as part of the quality control of the drugs. As no suitable monograph was available, the HPLC methods used were specifically validated in accordance with ICH Guideline Q2 and the EANM guideline. The validation results for linearity, accuracy, precision, specificity, LLOQ, LLOD, and carryover, obtained using both the radioactivity and UV detectors, are summarized in Table 2. The results demonstrate that the method is valid and yields accurate results. As only one HPLC instrument was used for quality control, no inter-instrument precision study was conducted. Instead, precision was assessed only between different analysts and days.

Table 2. Analytical HPLC validation parameters for [^{68}Ga]Ga-FAPi-mFS and [^{177}Lu]Lu-FAPi-mFS using UV and radioactivity detector.

	[^{68}Ga]GaFAPi-mFS	[^{nat}Ga]GaFAPi-mFS	[^{177}Lu]LuFAPi-mFS	[^{nat}Lu]LuFAPi-mFS
Linearity (min. 12 measurements, $R^2 > 0.99$)	Range from 75 kBq to 1250 kBq $R^2 = 0.9999$	Range from 30% to 160% $n = 3$ $R^2 = 0.9992$	Range from 2.5 MBq to 12.5 MBq $n = 3$ $R^2 = 0.9981$	Range from 30% to 160% $n = 3$ $R^2 = 0.9991$
Accuracy (recovery between 90 and 110%)	97.04 and 99.40%	96.69 and 101.34%	96.25 and 108.75%	97.76 and 101.05%
Precision (RSD < 1%)	RSD = 0.80	RSD = 0.08	RSD = 0.51	RSD = 0.04
Specificity (resolution > 1 between peaks)	t_R ([^{68}Ga]GaFAPi-mFS) = 4.03 min	t_R (unlabeled) = 4.95 min t_R (cold standard) = 4.00 min	t_R ([^{177}Lu]LuFAPi-mFS) = 5.37 min	t_R (unlabeled) = 4.50 min t_R (cold standard) = 5.29 min
Lower limit of detection	0.35 $\frac{kBq}{\mu L}$	69.12 $\frac{\mu g}{\mu L}$	0.63 $\frac{kBq}{\mu L}$	8.62 $\frac{\mu g}{\mu L}$
Lower limit of quantification	1.06 $\frac{kBq}{\mu L}$	209.46 $\frac{\mu g}{\mu L}$	1.91 $\frac{kBq}{\mu L}$	26.12 $\frac{\mu g}{\mu L}$

Stability studies using radio-TLC showed that the radiochemical purity of the ^{68}Ga-labeled tracer remained stable for 90 min and that of the ^{177}Lu-labeled tracer remained stable for 14 days, with no more than 11% of the metal being released (Figure 4). To further assess the stability of the drugs, HPLC measurements were performed 1 h after the synthesis was completed. Neither compound showed any significant changes in RCP, with values remaining above 95%. Studies on the long-term stability of the ^{177}Lu drug may be required for the centralized manufacture and distribution of [^{177}Lu]Lu-FAPi-mFS.

4. Materials and Methods

The precursor FAPi-mFS is commercially available from MedChemExpress. The reference standard [^{nat}Ga]Ga-FAPi-mFS and [^{nat}Lu]Lu-FAPi-mFS were produced in-house. The analytical data for both compounds are listed in supplemental information. Key resources are presented in Table 3.

Table 3. Key resources.

Reagent or Resource	Source	Identifier
FAPi-mFS	MedChemExpress	N/A
[^{nat}Ga]Ga- FAPi-mFS	Institute for Radiopharmaceutical Cancer Research at the Helmholtz Center Dresden-Rossendorf	N/A
[^{nat}Lu]Lu- FAPi-mFS	Institute for Radiopharmaceutical Cancer Research at the Helmholtz Center Dresden-Rossendorf	N/A
Ga-68 generator GalliaPharm	EZAG	N/A
[^{177}Lu]$LuCl_3$ n. c. a. EndolucinBeta	ITM	N/A
Excel Version 2610	Microsoft	https://www.microsoft.com/de-de/microsoft-365/excel (10 August 2026)
ChemDraw 12.0	Revvity Signals Software (Waltham, MA, USA)	https://revvitysignals.com/products/research/chemdraw (10 September 2026)
Agilent 1200 series HPLC	Agilent Technologies (Santa Clara, CA, USA)	https://www.agilent.com/en/product/liquid-chromatography (18 August 2026)

For radiolabeling, a stock solution with a concentration of 1 mg/mL, prepared using TraceSelect water (Sigma-Aldrich, St. Louis, MO, USA), was generally employed. All chemicals were of the highest available purity. HPLC solvents were purchased from Merck (Darmstadt, Germany) and were of HPLC grade. Reagents, materials, and low-contamination plastic cassettes were supplied by Trasis (Ans, Belgium). Bacterial endotoxin testing was conducted with a Nextgen PTS instrument (Charles River, Wilmington, MA, USA), using the corresponding disposable consumables. The radioactivity of the drug products was measured with an ISOMED2010 dose calibrator (NUVIA Instruments, Dülmen, Germany). Artificial intelligence in the form of Gemini and Perplexity was used for editing, linguistic revision, proofreading, and optimization. Figurelabs was used to create Figure 1.

Ga-68 was obtained by elution from a ^{68}Ge/^{68}Ga generator (GalliaPharm, Eckert & Ziegler Radiopharma GmbH, Berlin, Germany) and used directly without additional purification. For radiolabeling, 50 µg of precursor was combined with 2.0 mL of 1.0 M sodium acetate buffer (pH 5.5), and the reaction was carried out at 85 °C using an All-In-One Mini Synthesis Module (Trasis) equipped with a disposable cartridge. Subsequently, the reaction mixture was passed through an Oasis HLB-Plus cartridge, which had been preconditioned with 2 mL of ethanol and 5 mL of water, to remove free Ga-68. The product was eluted with 0.5 mL of ethanol. Finally, 10 mL of saline solution was added to dilute the product, which was then filtered through a sterile filter (Sterifix, B. Braun SE, Melsungen, Germany).

[^{177}Lu]$LuCl_3$ n.c.a. (EndolucinBeta) was supplied from ITM Isotope Technologies in Munich, Germany, at different activity concentrations in 0.04 M HCl (40 GBq/mL) and was used without additional purification. For radiolabeling, 1.2 mL of 0.6 M ascorbic acid solution including 30 mg gentisic acid and 20 mg L-methionine was used. The reaction was conducted at pH 4.5 and 40–60 µg of precursor per GBq of Lu-177 at 70 °C for 10 min followed by 50 °C for 40 min. An All-In-One Mini Synthesis Module (Trasis, Belgium) equipped with a disposable cassette was used. No further purification of the product was required. The final formulation was prepared by diluting with 15 mL of saline, followed by sterile filtration using a Sterifix filter (B. Braun SE, Germany). The pH was checked before and after radiolabeling using disposable pH strips (Merck, Germany). Reaction progress was monitored by radio-TLC (TLC Silicagel 60 F254, Merck, Germany) and two different mobile phases: (1) citrate buffer at pH 4 and (2) a 1:1 (*v*/*v*) mixture of 1.0 M ammonium acetate buffer and MeOH.

Analytical radio-HPLC was performed using an HPLC system (Agilent 1260 Infinity II, 100-µL injection loop, 20-µL injection for quality control) equipped with a GABI Nova radioactivity detector (Elysia-Raytest, Liège, Belgium) and an external mid-energy NaI(Tl)/photomultiplier tube (PMT) scintillation probe (Elysia-Raytest, Belgium). The following column was used: VDSpher PUR 150 C18-E 5 µm, 100 3 4.0 mm VDS Optilab, Germany. The mobile phases were acetonitrile (A) and water (B), each containing 0.1% TFA. The gradient, run at a flow rate of 1.0 mL/min, started at 10% A and increased to 20% A within 10 min for the Ga-68 labeled peptide and 20% A to 45% A within 10 min for the Lu-177 labeled peptide. The thin-layer chromatograms (TLCs) were analyzed using a miniGita TLC scanner (Elysia-Raytest, Belgium), and the data were evaluated using Gina analysis software Version 6.3 (Elysia-Raytest, Belgium).

HPLC analysis and preparative purification of [^{nat}Ga]Ga-FAPi-mFS and [^{nat}Lu]Lu-FAPi-mFS were performed out using a Knauer Azura system (Knauer, Berlin, Germany) equipped with a Synergi Hydro-RP column (4 µm, 80 Å, 250 × 10 mm). Analytical and preparative HPLC separations were performed at a flow rate of 5 mL min^{-1} using solvent A (H_2O containing 0.1% TFA) and solvent B (acetonitrile containing 0.1% TFA). The gradient was programmed from 5% to 55% B over 45 min.

High-resolution mass spectrometry (HRMS) analyses of [^{nat}Ga]Ga-FAPi-mFS and [^{nat}Lu]Lu-FAPi-mFS were performed on an Agilent Revident Q-TOF LC/MS G6575A instrument (Agilent Technologies, Waldbronn, Germany) equipped with an electrospray ionization (ESI) source and operated using Agilent MassHunter Workstation software (version 3.6). Measurements were conducted in bypass mode with a mobile phase consisting of solvent A (acetonitrile) and solvent B (0.1% formic acid in H_2O) at a flow rate of 0.2 mL min^{-1}.

The stability studies were conducted in triplicate at 37 °C in human serum (HS) and in the final product formulation. The HS (male AB plasma from the United States) was obtained from Sigma Aldrich (St. Louis, MO, USA). The saline solution was obtained from B. Braun (Germany). In the final step, 500 µL [^{68}Ga]Ga-FAPi-mFS of the formulated product solution (ca. 11 MBq) and for [^{177}Lu]Lu-FAPi-mFS 15 µL of the formulated product solution (48 MBq) was added to 1 mL of HS. Radio-TLC was performed under the analytical conditions mentioned above.

4.1. Quantification and Statistical Analysis

Gina Star software (Elysia-Raytest) was used to quantify the HPLC signals, and the signals were integrated manually. Excel (Microsoft) was used to analyze data. All numbers of replicates are specified in the paper and amount to at least n = 3 (number of

measurements). For the statistical analyses, the sample mean, standard deviation and linear regressions were used and calculated using Excel.

4.2. Experimental Details

4.2.1. Preparation of [^{nat}Ga]Ga-FAPi-mFS

A stock solution of FAPi-mFS (100 µL, 1 mM in H_2O) was mixed with 800 µL of 1.0 M sodium acetate buffer (pH 4.5), followed by the addition of 110 µL of a $Ga(NO_3)_3$ solution (1 mM in sodium acetate buffer). The reaction mixture was incubated at 80 °C for 20 min with continuous shaking at 700 rpm. Upon completion, the reaction was analyzed by HPLC, which confirmed quantitative conversion of FAPi-mFS to the desired product. The product fraction was subsequently collected and characterized by high-resolution mass spectrometry (HRMS). [^{nat}Ga]Ga-FAPi-mFS: HPLC, t_n = 25.86 min. HRMS (ESI-QTOF) m/z calculated for $[M + Ga\text{-}H]^{2+}$ 635.1923; found 635.1921 (where M = $C_{53}H_{69}F_3N_{12}O_{15}S$, FAPi-mFS).

4.2.2. Preparation of [^{nat}Lu]Lu-FAPi-mFS

A stock solution of FAPi-mFS (100 µL, 1 mM in H_2O) was mixed with 800 µL of 1.0 M sodium acetate buffer (pH 4.5), followed by the addition of 110 µL of a $LuCl_3$ solution (1 mM in sodium acetate buffer). The reaction mixture was incubated at 80 °C for 30 min with continuous shaking at 700 rpm. After completion of the reaction, HPLC confirmed quantitative conversion of FAPi-mFS to the corresponding Lu complex. The product was isolated by HPLC purification and subsequently characterized by high-resolution mass spectrometry (HRMS). [^{nat}Lu]Lu-FAPi-mFS: HPLC, t_n = 25.98 min. HRMS (ESI-QTOF) m/z calculated for $[M + Lu\text{-}2H]^+$ 1375.3924; found 1375.3925, calculated for $[M + Lu\text{-}H]^{2+}$ 688.1999; found 688.2000 (where M = $C_{53}H_{69}F_3N_{12}O_{15}S$, FAPi-mFS).

5. Conclusions

Automated labeling procedures for [^{68}Ga]Ga-FAPi-mFS and [^{177}Lu]Lu-FAPi-mFS were successfully developed, optimized, and validated. Both procedures enabled reproducible production with high radiochemical purity and sufficient in vitro stability. In addition, robust radio-HPLC methods were established and validated for routine quality control, demonstrating adequate linearity, accuracy, precision, specificity, and sensitivity. As covalent, FAP-specific radiopharmaceuticals, both compounds represent promising candidates for further clinical evaluation, with the potential to prolong tumor retention and improve the efficacy of FAP-specific imaging as well as radionuclide therapy.

Supplementary Materials: The following supporting information can be downloaded at https://www.mdpi.com/article/10.3390/ph19111707/s1. Figure S1: Radio-HPLC chromatogram of [^{177}Lu]Lu-FAPi-mFS after labeling at 85 °C for 40 min, where the desired product peak has a t_R of 5.57 min and the peak of the major side product a t_R of 4.47 min (17.5%). For better presentation, a different method was used (method: gradient from 5% to 95% MeCN + 0.1% TFA in 10 min); Figure S2: Specificity measurements for UV unlabeled peptide FAPi-mFS (UV trace), in green, and non-radioactive [^{nat}Ga]Ga-FAPi-mFS (UV trace), in red (Materials and Methods section); Figure S3: Specificity measurements for UV and radiodetector, showing unlabeled FAPi-mFS (UV trace) in red, non-radioactive [^{nat}Lu]Lu-FAPi-mFS (UV trace) in blue and drug product [^{177}Lu]Lu-FAPi-mFS (radioactivity trace) in green (Materials and Methods section); Figure S4: Carryover measurement of [^{68}Ga]Ga-FAPi-mFS on analytical HPLC performed after 15 consecutive injections of [^{68}Ga]Ga-FAPi-mFS at high activities (Materials and Methods section); Figure S5: Carryover measurement of [^{177}Lu]Lu-FAPi-mFS on analytical HPLC performed after six consecutive injections of [^{177}Lu]Lu-FAPi-mFS at high activities (Materials and Methods section); Figure S6: HPLC data from FAPi-mFS (Materials and Methods section); Figure S7: HPLC data from [^{nat}Ga]GaFAPi-mFS (Materials and

Methods section); Figure S8: HPLC data from [^{nat}Lu]LuFAPi-mFS (Materials and Methods section); Figure S9: HRMS data from FAPi-mFS, provided by the Institute for Radiopharmaceutical Cancer Research at the Helmholtz Center Dresden-Rossendorf (Materials and Methods section); Figure S10: HRMS data from [^{nat}Ga]GaFAPi-mFS, provided by the Institute for Radiopharmaceutical Cancer Research at the Helmholtz Center Dresden-Rossendorf (Materials and Methods section); Figure S11: HRMS data from [^{nat}Lu]LuFAPi-mFS, provided by the Institute for Radiopharmaceutical Cancer Research at the Helmholtz Center Dresden-Rossendorf (Materials and Methods section).

Author Contributions: Conceptualization, S.S. (Sarah Stephan), L.G. and R.P.B.; methodology, S.S. (Sarah Stephan) and L.G.; software, S.S. (Sarah Stephan), S.P., S.S. (Sven Stadlbauer) and L.G.; validation, S.S. (Sarah Stephan) and L.G.; formal analysis, S.S. (Sarah Stephan), S.P., S.S. (Sven Stadlbauer) and L.G.; investigation, S.S. (Sarah Stephan), S.P., S.S. (Sven Stadlbauer), A.E., R.L., C.L., R.P.B. and L.G.; resources, R.L., C.L. and R.P.B.; data curation, R.L., C.L. and R.P.B.; writing—original draft preparation, S.S. (Sarah Stephan), S.P. and L.G.; writing—review and editing, S.S. (Sven Stadlbauer), A.E., R.L., C.L. and R.P.B.; visualization, S.S. (Sarah Stephan) and L.G.; supervision, R.P.B. All authors have read and agreed to the published version of the manuscript.

Funding: This research received no external funding.

Institutional Review Board Statement: Not applicable.

Informed Consent Statement: Not applicable.

Data Availability Statement: The original contributions presented in this study are included in the article/Supplementary Material. Further inquiries can be directed to the corresponding authors.

Acknowledgments: Special thanks to the team at Curanosticum Wiesbaden-Frankfurt (Wiesbaden, Germany). During the preparation of this manuscript, the author(s) used Figurelabs.ai (https://www.figurelabs.ai/), accessed on May 2026 for the purposes of creating Figure 1. The authors have reviewed and edited the output and take full responsibility for the content of this publication.

Conflicts of Interest: Sarah Stephan, Aleksandr Eismant, Rimos Lahdo, Christian Landvogt, Richard P. Baum and Lukas Greifenstein are either employed by the company Curanosticum MVZ GmbH Wiesbaden-Frankfurt or are owners of the same. The remaining authors declare that the research was conducted in the absence of any commercial or financial relationships that could be construed as a potential conflict of interest.

Abbreviations

The following abbreviations are used in this manuscript:

FAP	fibroblast activation protein
CTR	covalent targeted radioligand
SuFEx	sulfur(VI) fluoride exchange
PET	positron emission tomography
CAF	cancer-associated fibroblast
Ga-68	gallium-68
Lu-177	lutetium-177
HCl	hydrochloric acid
NaCl	sodium chloride
HPLC	high-performance liquid chromatography
TLC	thin-layer chromatography
RCY	decay-corrected radiochemical yield
RCP	radiochemical purity
MeCN	acetonitrile
TFA	trifluoroacetic acid
MeOH	methanol
HS	human serum

ICH	International Council for Harmonisation of Technical Requirements for Pharmaceuticals for Human Use
EANM	European Association of Nuclear Medicine
LLOD	lower limit of detection
LLOQ	lower limit of quantification
RSD	relative standard deviation
UV	ultraviolet
HRMS	high-resolution mass spectrometry

References

1. De Decker, A.; Vliegen, G.; Van Rompaey, D.; Peeraer, A.; Bracke, A.; Verckist, L.; Jansen, K.; Geiss-Friedlander, R.; Augustyns, K.; De Winter, H.; et al. Novel Small Molecule-Derived, Highly Selective Substrates for Fibroblast Activation Protein (FAP). *ACS Med. Chem. Lett.* **2019**, *10*, 1173–1179. [CrossRef] [PubMed]
2. Hamson, E.J.; Keane, F.M.; Tholen, S.; Schilling, O.; Gorrell, M.D. Understanding fibroblast activation protein (FAP): Substrates, activities, expression and targeting for cancer therapy. *Proteom. Clin. Appl.* **2014**, *8*, 454–463. [CrossRef] [PubMed]
3. Kratochwil, C.; Flechsig, P.; Lindner, T.; Abderrahim, L.; Altmann, A.; Mier, W.; Adeberg, S.; Rathke, H.; Röhrich, M.; Winter, H.; et al. Ga-FAPI PET/CT: Tracer Uptake in 28 Different Kinds of Cancer. *J. Nucl. Med.* **2019**, *60*, 801–805. [CrossRef] [PubMed]
4. Loktev, A.; Lindner, T.; Burger, E.-M.; Altmann, A.; Giesel, F.; Kratochwil, C.; Debus, J.; Marmé, F.; Jäger, D.; Mier, W.; et al. Development of Fibroblast Activation Protein–Targeted Radiotracers with Improved Tumor Retention. *J. Nucl. Med.* **2019**, *60*, 1421–1429. [CrossRef] [PubMed]
5. Sollini, M.; Kirienko, M.; Gelardi, F.; Fiz, F.; Gozzi, N.; Chiti, A. State-of-the-art of FAPI-PET imaging: A systematic review and meta-analysis. *Eur. J. Nucl. Med. Mol. Imaging* **2021**, *48*, 4396–4414. [CrossRef] [PubMed]
6. Gilardi, L.; Airò Farulla, L.S.; Demirci, E.; Clerici, I.; Omodeo Salè, E.; Ceci, F. Imaging Cancer-Associated Fibroblasts (CAFs) with FAPi PET. *Biomedicines* **2022**, *10*, 523. [CrossRef] [PubMed]
7. Ryabtsova, O.; Jansen, K.; Van Goethem, S.; Joossens, J.; Cheng, J.D.; Lambeir, A.-M.; De Meester, I.; Augustyns, K.; Van der Veken, P. Acylated Gly-(2-cyano)pyrrolidines as inhibitors of fibroblast activation protein (FAP) and the issue of FAP/prolyl oligopeptidase (PREP)-selectivity. *Bioorg. Med. Chem. Lett.* **2012**, *22*, 3412–3417. [CrossRef] [PubMed]
8. Mattiussi, S.; Herth, M.M.; Battisti, U.M. Advancing fibroblast activation protein inhibitors for targeted radioligand therapy: Strategies and innovations to increase tumor residence time. *Eur. J. Med. Chem.* **2026**, *309*, 118737. [CrossRef] [PubMed]
9. Lindner, T.; Giesel, F.L.; Kratochwil, C.; Serfling, S.E. Radioligands Targeting Fibroblast Activation Protein (FAP). *Cancers* **2021**, *13*, 5744. [CrossRef] [PubMed]
10. Zhong, X.; Guo, J.; Han, X.; Wu, W.; Yang, R.; Zhang, J.; Shao, G. Synthesis and Preclinical Evaluation of a Novel FAPI-04 Dimer for Cancer Theranostics. *Mol. Pharm.* **2023**, *20*, 2402–2414. [CrossRef] [PubMed]
11. Giesel, F.L.; Kratochwil, C.; Lindner, T.; Marschalek, M.M.; Loktev, A.; Lehnert, W.; Debus, J.; Jäger, D.; Flechsig, P.; Altmann, A.; et al. Ga-FAPI PET/CT: Biodistribution and Preliminary Dosimetry Estimate of 2 DOTA-Containing FAP-Targeting Agents in Patients with Various Cancers. *J. Nucl. Med.* **2019**, *60*, 386–392. [CrossRef] [PubMed]
12. Fendler, W.P.; Pabst, K.M.; Kessler, L.; Fragoso Costa, P.; Ferdinandus, J.; Weber, M.; Lippert, M.; Lueckerath, K.; Umutlu, L.; Kostbade, K. Safety and efficacy of 90Y-FAPI-46 radioligand therapy in patients with advanced sarcoma and other cancer entities. *Clin. Cancer Res.* **2022**, *28*, 4346–4353. [CrossRef] [PubMed]
13. Fendler, W.P.; Bartel, T.; Pabst, K.M.; Hamacher, R.; Hirmas, N.; Seifert, R.; Kasper, S.; Nader, M.; Kesch, C.; Tresckow, B.V.; et al. ^{68}Ga-FAPI-46 PET for cancer imaging: A prospective single-arm clinical trial. *J. Clin. Oncol.* **2023**, *41*, 3064. [CrossRef]
14. Ferdinandus, J.; Costa, P.F.; Kessler, L.; Weber, M.; Hirmas, N.; Kostbade, K.; Bauer, S.; Schuler, M.; Ahrens, M.; Schildhaus, H.-U. Initial clinical experience with 90Y-FAPI-46 radioligand therapy for advanced-stage solid tumors: A case series of 9 patients. *J. Nucl. Med.* **2022**, *63*, 727–734. [CrossRef] [PubMed]
15. Helisch, A.; Kratochwil, C.; Kleist, C.; Krämer, S.; Rosales Castillo, J.J.; Dendl, K.; Rathke, H.; von Goetze, I.; Schreckenberger, M.; Jäger, D.; et al. Feasibility, Tolerability, and Preliminary Clinical Response of Fractionated Radiopharmaceutical Therapy with ^{213}Bi-FAPI-46: Pilot Experience in Patients with End-Stage, Progressive Metastatic Tumors. *J. Nucl. Med.* **2024**, *65*, 1917–1922. [CrossRef] [PubMed]
16. Liu, Y.; Watabe, T.; Kaneda-Nakashima, K.; Shirakami, Y.; Naka, S.; Ooe, K.; Toyoshima, A.; Nagata, K.; Haberkorn, U.; Kratochwil, C.; et al. Fibroblast activation protein targeted therapy using [177Lu]FAPI-46 compared with [225Ac]FAPI-46 in a pancreatic cancer model. *Eur. J. Nucl. Med. Mol. Imaging* **2022**, *49*, 871–880. [CrossRef] [PubMed]
17. Moon, E.S.; Elvas, F.; Vliegen, G.; De Lombaerde, S.; Vangestel, C.; De Bruycker, S.; Bracke, A.; Eppard, E.; Greifenstein, L.; Klasen, B. Targeting fibroblast activation protein (FAP): Next generation PET radiotracers using squaramide coupled bifunctional DOTA and DATA5m chelators. *EJNMMI Radiopharm. Chem.* **2020**, *5*, 19. [CrossRef] [PubMed]

18. Moon, E.S.; Ballal, S.; Yadav, M.P.; Bal, C.; Van Rymenant, Y.; Stephan, S.; Bracke, A.; Van der Veken, P.; De Meester, I.; Roesch, F. Fibroblast activation protein (FAP) targeting homodimeric FAP inhibitor radiotheranostics: A step to improve tumor uptake and retention time. *Am. J. Nucl. Med. Mol. Imaging* **2021**, *11*, 476. [PubMed]
19. Greifenstein, L.; Kramer, C.S.; Moon, E.S.; Rösch, F.; Klega, A.; Landvogt, C.; Müller, C.; Baum, R.P. From Automated Synthesis to In Vivo Application in Multiple Types of Cancer—Clinical Results with [68Ga]Ga-DATA5m. SA.FAPi. *Pharmaceuticals* **2022**, *15*, 1000. [CrossRef] [PubMed]
20. Ballal, S.; Yadav, M.P.; Moon, E.S.; Kramer, V.S.; Roesch, F.; Kumari, S.; Bal, C. First-In-Human Results on the Biodistribution, Pharmacokinetics, and Dosimetry of [177Lu]Lu-DOTA.SA.FAPi and [177Lu]Lu-DOTAGA. (SA.FAPi)2. *Pharmaceuticals* **2021**, *14*, 1212. [CrossRef] [PubMed]
21. Kreppel, B.; Gärtner, F.C.; Marinova, M.; Attenberger, U.; Meisenheimer, M.; Toma, M.; Kristiansen, G.; Feldmann, G.; Moon, E.S.; Roesch, F. [68Ga]Ga-DATA5m. SA. FAPi PET/CT: Specific tracer-uptake in focal nodular hyperplasia and potential role in liver tumor imaging. *Nukl.-Nucl.* **2020**, *59*, 387–389. [CrossRef] [PubMed]
22. Galbiati, A.; Zana, A.; Bocci, M.; Millul, J.; Elsayed, A.; Mock, J.; Neri, D.; Cazzamalli, S. A Dimeric FAP-Targeting Small-Molecule Radioconjugate with High and Prolonged Tumor Uptake. *J. Nucl. Med.* **2022**, *63*, 1852–1858. [CrossRef] [PubMed]
23. Galbiati, A.; Bocci, M.; Ravazza, D.; Mock, J.; Gilardoni, E.; Neri, D.; Cazzamalli, S. Preclinical Evaluation of ^{177}Lu-OncoFAP-23, a Multivalent FAP-Targeted Radiopharmaceutical Therapeutic for Solid Tumors. *J. Nucl. Med.* **2024**, *65*, 1604–1610. [CrossRef] [PubMed]
24. Xu, M.; Zhang, P.; Ding, J.; Chen, J.; Huo, L.; Liu, Z. Albumin Binder-Conjugated Fibroblast Activation Protein Inhibitor Radiopharmaceuticals for Cancer Therapy. *J. Nucl. Med.* **2022**, *63*, 952–958. [CrossRef] [PubMed]
25. Wen, X.; Xu, P.; Shi, M.; Liu, J.; Zeng, X.; Zhang, Y.; Shi, C.; Li, J.; Guo, Z.; Zhang, X.; et al. Evans blue-modified radiolabeled fibroblast activation protein inhibitor as long-acting cancer therapeutics. *Theranostics* **2022**, *12*, 422–433. [CrossRef] [PubMed]
26. Zhou, H.; Zhong, J.; Liu, Y.; Peng, S.; Yan, Q.; Wang, L.; Zhong, Y.; Hu, K. Development of ibuprofen-modified fibroblast activation protein radioligands to improve cancer therapy. *Eur. J. Med. Chem.* **2025**, *283*, 117115. [CrossRef] [PubMed]
27. Greifenstein, L.; Martin, M.; Kramer, C.; Klega, A.; Mueller, C.; Landvogt, C.; Hoehne, A.; Osterkamp, F.; Smerling, C.; Rösch, F.; et al. Radiolabeling of 3BP-3940 with 68Ga, 90Y. *J. Nucl. Med.* **2022**, *63*, 2532.
28. Zboralski, D.; Hoehne, A.; Bredenbeck, A.; Schumann, A.; Nguyen, M.; Schneider, E.; Ungewiss, J.; Paschke, M.; Haase, C.; von Hacht, J.L.; et al. Preclinical evaluation of FAP-2286 for fibroblast activation protein targeted radionuclide imaging and therapy. *Eur. J. Nucl. Med. Mol. Imaging* **2022**, *49*, 3651–3667. [CrossRef] [PubMed]
29. Zboralski, D.; Osterkamp, F.; von Hacht, J.L.; Bredenbeck, A.; Höhne, A.; Libera-Körner, J.; Ungewiss, J.; Paschke, M.; Reineke, U.; Smerling, C. Preclinical Development of 3BP-3940, a Fibroblast Activation Protein–Targeted Cyclic Peptide–Based Radiotheranostic for Imaging and Therapy. *J. Nucl. Med.* **2026**, *67*, 594–600. [CrossRef] [PubMed]
30. Baum, R.P.; Schuchardt, C.; Singh, A.; Chantadisai, M.; Robiller, F.C.; Zhang, J.; Mueller, D.; Eismant, A.; Almaguel, F.; Zboralski, D.; et al. Feasibility, Biodistribution, and Preliminary Dosimetry in Peptide-Targeted Radionuclide Therapy of Diverse Adenocarcinomas Using ^{177}Lu-FAP-2286: First-in-Humans Results. *J. Nucl. Med.* **2022**, *63*, 415–423. [CrossRef] [PubMed]
31. Pang, Y.; Zhao, L.; Meng, T.; Xu, W.; Lin, Q.; Wu, H.; Zhang, J.; Chen, X.; Sun, L.; Chen, H. PET Imaging of Fibroblast Activation Protein in Various Types of Cancer Using ^{68}Ga-FAP-2286: Comparison with ^{18}F-FDG and ^{68}Ga-FAPI-46 in a Single-Center, Prospective Study. *J. Nucl. Med.* **2023**, *64*, 386–394. [CrossRef] [PubMed]
32. Baum, R.P.; Novruzov, E.; Zhao, T.; Greifenstein, L.; Jakobsson, V.; Perrone, E.; Mishra, A.; Eismant, A.; Ghai, K.; Klein, O.; et al. Radiomolecular Theranostics With Fibroblast-Activation-Protein Inhibitors and Peptides. *Semin. Nucl. Med.* **2024**, *54*, 537–556. [CrossRef] [PubMed]
33. Cui, X.-Y.; Li, Z.; Kong, Z.; Liu, Y.; Meng, H.; Wen, Z.; Wang, C.; Chen, J.; Xu, M.; Li, Y.; et al. Covalent targeted radioligands potentiate radionuclide therapy. *Nature* **2024**, *630*, 206–213. [CrossRef] [PubMed]
34. Kong, Z.; Li, Z.; Cui, X.Y.; Wang, J.; Xu, M.; Liu, Y.; Chen, J.; Ni, S.; Zhang, Z.; Fan, X.; et al. CTR-FAPI PET Enables Precision Management of Medullary Thyroid Carcinoma. *Cancer Discov.* **2025**, *15*, 316–328. [CrossRef] [PubMed]
35. Gillings, N.; Todde, S.; Behe, M.; Decristoforo, C.; Elsinga, P.; Ferrari, V.; Hjelstuen, O.; Peitl, P.K.; Koziorowski, J.; Laverman, P. EANM guideline on the validation of analytical methods for radiopharmaceuticals. *EJNMMI Radiopharm. Chem.* **2020**, *5*, 7. [CrossRef] [PubMed]
36. De Decker, M.; Turner, J.H. Automated Module Radiolabeling of Peptides and Antibodies with Gallium-68, Lutetium-177 and Iodine-131. *Cancer Biother. Radiopharm.* **2012**, *27*, 72–76. [CrossRef] [PubMed]
37. Iori, M.; Capponi, P.C.; Rubagotti, S.; Esposizione, L.R.; Seemann, J.; Pitzschler, R.; Dreger, T.; Formisano, D.; Grassi, E.; Fioroni, F.; et al. Labelling of 90Y- and 177Lu-DOTA-Bioconjugates for Targeted Radionuclide Therapy: A Comparison among Manual, Semiautomated, and Fully Automated Synthesis. *Contrast Media Mol. Imaging* **2017**, *2017*, 8160134. [CrossRef] [PubMed]

Disclaimer/Publisher's Note: The statements, opinions and data contained in all publications are solely those of the individual author(s) and contributor(s) and not of MDPI and/or the editor(s). MDPI and/or the editor(s) disclaim responsibility for any injury to people or property resulting from any ideas, methods, instructions or products referred to in the content.